Theor Chem Acc (2010) 127:587–594
DOI 10.1007/s00214-010-0752-4

REGULAR ARTICLE

Theoretical investigations of the charge transfer properties of anthracene derivatives

Ahmad Irfan · Jingping Zhang · Yingfei Chang

Received: 8 January 2010 / Accepted: 27 March 2010 / Published online: 14 April 2010

Abstract The simulated structure of 9,10-bis(methylthio)anthracene (**1**) has been compared with experimental parameters, then by applying the same methodology crystal structures of designed derivatives 9,10-bis(trifluoromethylthio)anthracene (**2**), 9,10-bis(methylselleno)anthracene (**3**) and 9,10-bis(trifluoromethylselleno)anthracene (**4**) have been simulated. By employing a diabatic model and a first-principle direct method, we have investigated carrier transport properties. The reorganization energies have been computed at the DFT (B3LYP/6-31G*) level. The transfer integrals have been calculated for a wide variety of nearest-neighbor charge transfer pathways. The reorganization energies and transfer integrals showed that **1**, **3**, and **4** would be good both for hole and electron transport and **2** hole transfer material. The **2** and **4** derivatives would enhance the photostability as well.

Keywords OFET · Reorganization energy · Transfer integrals · DFT · Anthracene derivatives

1 Introduction

Organic materials are good contenders for the fabrication of transistors, photodiodes, solar cells, and (bio)chemical sensors [1–4]. Since the reporting of the first organic field effect transistor (OFET) [5] in 1986, there has been remarkable progress in the development of OFETs. Intermolecular and intramolecular interactions are known to have important influence on the structures, properties, and reactivity of certain chalcogen compounds [6, 7]. Compounds containing chalcogen atoms (S, Se, and Te) are a treasury of molecular electronics, e.g., OFET [8, 9]. Solid-state properties such as conductivity, reactivity, and crystallinity all rely on influences of π–π forces [10]. Realization of a 2-D face-to-face π–π stacked packing arrangement of acenes would produce improved OFET devices with a high hole mobility [11, 12] because this molecular ordering permits good overlapping of the intermolecular π–π orbitals.

Kobayashi et al. [13] reported that chalcogen–chalcogen interaction plays an important role in the face-to-face π–π stacking arrangement. The 9,10-bis(methylthio)anthracene (**1**) has been selected to calculate the charge transfer properties which is aligned by face-to-face π–π stacking. Computational techniques [14, 15] have become in the past decades a potential alternative to experiments for investigation of single-component systems. The reorganization energy and transfer integrals are important parameters of the mobility. If the crystal structure is not available, then transfer integrals are generally calculated within the dimer by intermolecular separation, translation distance along axis (X, Y and Z), and change in rotational angle, but this method does not give accurate predictions relative to crystal structure [16–18]. The molecular mechanics has been applied to crystal surfaces or to the bulk [19], allow determination of how molecular species assemble in the solid state. Molecular mechanics simulations have been used to optimize the conformation and crystal packings [20]. The crystal parameters have been successfully regenerated by molecular mechanics minimizations [21].

Electronic supplementary material The online version of this article (doi:10.1007/s00214-010-0752-4) contains supplementary material, which is available to authorized users.

A. Irfan · J. Zhang (✉) · Y. Chang
Faculty of Chemistry, Northeast Normal University, Changchun 130024, China
e-mail: zhangjingping66@yahoo.com.cn

The high mobility materials having face-to-face π–π stacking arrangement were designed. The crystal structures of the designed systems are not available; thus we have simulated the crystal structures to calculate the transfer integrals. In this work, our aims are (a) to design high mobility photostable materials; it is expected that electron withdrawing character of fluorine substituents may improve the photostability [22]. Thus, we have substituted the H by electron-withdrawing group F atoms. (b) To theoretically investigate the carrier transport properties of studied systems (see Fig. 1).

2 Theoretical background and methodology

The initial molecular structures were taken from density functional theory (DFT) geometry optimizations using Becke's exchange functional [23] combined with Lee–Yang–Parr correlation functional [24], denoted B3LYP [25] at the 6-31G* and 6-31G** basis sets [14]. It has been found that the B3LYP/6-31G* level gives accurate and reasonable results (see supporting information). The forcite code which is implemented in the Accelrys package Materials Studio is used to simulate the crystal structure of 9,10-bis(methylthio)anthracene (**1**) [26]. The geometry of the cluster models used in present study was taken from B3LYP/6-31G* level. In this paper, the potential parameters are selected from the Dreiding, which has been fully validated by many works [27–30]. The Dreiding force field, developed by Mayo et al. [30] is a good, all-purpose force field that can be used for organic, biological, and main-group inorganic molecules. The geometry constraints were applied during dreiding energy minimization. The electrostatic interaction is evaluated through the Ewald sum method [31]. The structural parameters were compared with experimental data to check the reliability of simulated structure. Then the designed derivatives were optimized at the B3LYP/6-31G* level. The geometric characters of compounds **2**–**4** are very similar to that of compound **1**. Thus, by applying the above-mentioned methodology crystal structures of new designed derivatives have been simulated within $P\bar{1}$ space group to relate the pathways in the different structures, and discuss how the substituents affect the transfer integrals of the same pathway in the different structures. In fact, we would speculate that for compounds **2** and **4** the actual crystal structures may be different, since the C–F bonds are in the place of C–H bonds of other compounds. But from simulated crystal structures, we would be able to check the effect of substituents on the transfer integrals. Second, it can give us idea as to what kind of charge transfer properties would have such kind of materials.

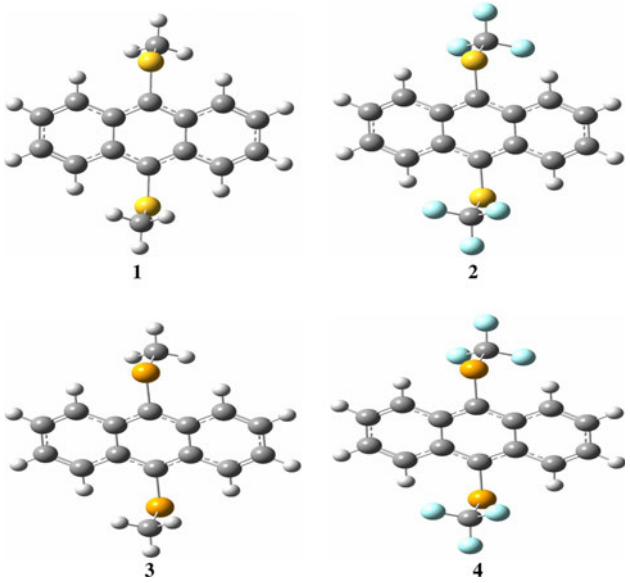

Fig. 1 The structures of 9,10-bis(methylthio)anthracene (**1**), 9,10-bis(trifluoromethylthio)anthracene (**2**), 9,10-bis(methylselleno)anthracene (**3**), 9,10-bis(trifluoromethylselleno)anthracene (**4**)

The charge transport in the organic solid can be viewed as hopping process, which can be accounted for by the Marcus electron transfer theory [32]. For self-exchange transfer reaction, the driven force, i.e., the free energy difference (ΔG^0) is approximately taken as zero in the transfer. As result, the transfer rate constant is represented as

$$k = V^2/\mathrm{h}(\pi/\lambda k_\mathrm{B}T)^{1/2}\exp(-\lambda/4k_\mathrm{B}T) \quad (1)$$

Here, V is the intermolecular transfer integral and λ is the reorganization energy. The reorganization energy is further divided into two parts: $\lambda_{\mathrm{rel}}^{(1)}$ and $\lambda_{\mathrm{rel}}^{(2)}$, where $\lambda_{\mathrm{rel}}^{(1)}$ corresponds to the geometry relaxation energy of one molecule from neutral state to charged state, and $\lambda_{\mathrm{rel}}^{(2)}$ corresponds to the geometry relaxation energy from charged state to neutral one [33, 34].

$$\lambda = \lambda_{\mathrm{rel}}^{(1)} + \lambda_{\mathrm{rel}}^{(2)} \quad (2)$$

In the evaluation of λ, the two terms were computed directly from the adiabatic potential energy surfaces; see Fig. 2 [14, 35, 36].

$$\begin{aligned}\lambda &= \lambda_{\mathrm{rel}}^{(1)} + \lambda_{\mathrm{rel}}^{(2)} \\ &= [E^{(1)}(X^+) - E^{(0)}(X^+)] + [E^{(1)}(X) - E^{(0)}(X)]\end{aligned} \quad (3)$$

Here, $E^{(0)}(X)$, $E^{(0)}(X^+)$ are the ground-state energies of the neutral and charged states, $E^{(1)}(X)$ is the energy of the neutral molecule at the optimized charged geometry, and $E^{(1)}(X^+)$ is the energy of the charged state at the geometry of the optimized neutral molecule.

We calculated the reorganization energy of anthracene at the B3LYP/6-31G*, B3LYP/6-31G** [14], and B3LYP/

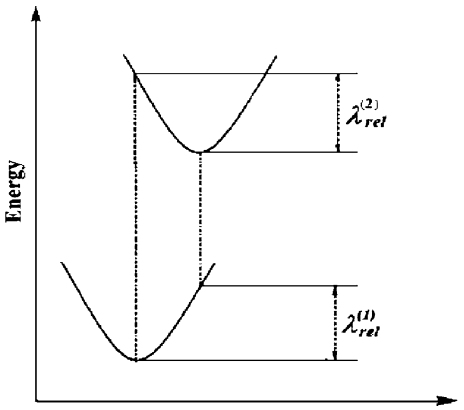

Fig. 2 Sketch for the potential energy surfaces for neutral state *1* and ionic state *2*, showing the vertical transitions and relaxation energies $\lambda_{\mathrm{rel}}^{(1)}$ and $\lambda_{\mathrm{rel}}^{(2)}$

6-31 + G* levels of theory. The B3LYP/6-31G* level gives reasonable results; thus, this level has been applied to compute the reorganization energies of its derivatives investigated here. It should be pointed out that, in this work, the polarization effects from the surrounding molecules, as well as the charge reorientation, have been neglected [37–39]. The next step is to calculate the transfer integrals. Here, we have used the single-crystal structures to generate all the possible nearest-neighbor intermolecular hopping pathways. The electronic coupling can be obtained either by Koopmans' theorem, which has been widely employed [40], or by directly evaluating the coupling element for the frontier orbitals [41, 42]. In the former case, the charge transfer integral corresponds to half of the splitting of the HOMO or LUMO levels for holes or electrons. Bredas et al. [14] have extensively investigated the parameters governing the transport on many conjugated systems by frontier orbital splitting. INDO based calculations which use the "energy-splitting-in-dimer" method [43] often overestimate electronic couplings and also ignore the orthogonalisation of the basis set. Valeev et al. [43] pointed out that when the dimer is not cofacially stacked, the site-energy correction due to the crystal environment should be taken into account. Yang et al. [44] have mentioned that the direct method for the coupling is equivalent to the site-energy corrected frontier orbital splitting method, and this direct method offers remarkable simplicity in computation; thus, we used direct method which has been proved to give good and accurate results [41, 42, 44–47].

The electronic coupling for electron/hole transfer in this scheme can be written as

$$\left\langle V = t_{\mathrm{e/h}} = \phi_{\mathrm{LUMO/HOMO}}^{0,\mathrm{site1}} | F^0 | \phi_{\mathrm{LUMO/HOMO}}^{0,\mathrm{site2}} \right\rangle \quad (4)$$

Here, V is the transfer integral for the hole or electron and $\phi_{\mathrm{LUMO/HOMO}}^{0,\mathrm{site1}}$ and $\phi_{\mathrm{LUMO/HOMO}}^{0,\mathrm{site2}}$ represent the LUMOs/HOMOs of the two adjacent molecules 1 and 2 when no intermolecular interaction is presented. F^0 is the Kohn–Sham–Fock matrix for the dimer; its density matrix is constructed from non-interacting molecular orbitals. In practice, the Fockmatrix is evaluated as

$$F = SC\varepsilon C^{-1} \quad (5)$$

Here, S is the overlap matrix for the dimer taken from the crystal structure, and the Kohn–Sham orbital C and eigenvalue ε are obtained by diagonalizing the zeroth-order Fock matrix without any self-consistent field iteration. In the present study transfer integrals have been computed at the DFT/pw91pw91/6-31G* level [44]. It has been revealed that this choice of functional gives the best results at the DFT level [48]. Furthermore, in organic materials intermolecular charge transfer rate between different dimers can vary by orders of magnitudes. The grain boundaries are present in thin film phases. Such inhomogeneities point out the inadequacy of diffusion constant to describe actual materials [49].

In the presence of such inhomogeneities, random walk approach can be performed to simulate the diffusion process of the charge carrier. Within this approach, an arbitrary site (molecule) within the bulk is initially chosen as the starting position for the charge [50, 51].

If we assume the charge motion is a homogeneous random walk, the diffusion constant can be evaluated as [52]

$$D = \lim_{t\to\infty} \frac{1}{2n} \frac{<x(t)^2>}{t} \approx \frac{1}{2n} \sum_i d_i^2 k_i p_i = \frac{1}{2n} \frac{\sum_i d_i^2 k_i^2}{\sum_i k_i} \quad (6)$$

d is the intermolecular center-to-center distance and $n = 3$ is the spatial dimension. The hopping time between two adjacent molecules is the inverse of the rate constant $1/k$. The probability for a specific hopping route is $p_i = \frac{k_i}{\sum_i k_i}$. Namely, it is a 3-d averaged diffusion process. It is clear that the mobility is linearly proportional to the electron transfer rate. Within this mechanism, it has been assumed that the localized electron can only hop between adjacent molecules, in sharp contrast to the band-like picture, where the electron is delocalized in several molecules. All the quantum chemistry calculations are performed with the Gaussian03 package [53].

3 Results and discussion

3.1 Molecular packing

Table 1 lists the cell parameters (a, b, and c: Å and α, β, and γ: °) using dreiding force field. As we have designed some new derivatives and wanted to calculate the charge

Table 1 Molecular packings of the studied systems

Parameters Space group	**1**[a] $P\bar{1}$	**1**[b] $P\bar{1}$	**2**	**3**	**4**
a (Å)	5.195	5.252	5.491	6.153	5.628
b (Å)	7.458	7.539	7.653	7.318	7.848
c (Å)	9.002	9.262	9.640	8.591	9.328
α (deg)	74.066	73.599	70.319	80.304	75.331
β (deg)	73.691	76.366	82.375	68.330	78.900
γ (deg)	89.762	88.184	83.855	91.632	86.183

[a] Experimental data from [13]

[b] Simulated crystal structure parameters where initial molecule was optimized at B3LYP/6-31G* level

transfer properties, thus, before simulating the crystal structures of designed derivatives, we have simulated the crystal parameters of the **1** which was initially optimized at the B3LYP/6-31G* level. It has been observed that unit cell of **1** shows $P\bar{1}$ space group with $a = 5.205$ Å, $b = 7.585$ Å, $c = 8.710$ Å, $\alpha = 76.500°$, $\beta = 75.540°$ and $\gamma = 90.730°$ which is in good agreement with experimental parameters [13]. The experimental crystal structure was successfully generated by forcite calculations. In Fig. 3 experimental and simulated crystal structures can be viewed. It has been observed that arrangement and orientation of the molecules in simulated crystal is also similar like the experimental one. Our adopted methodology is

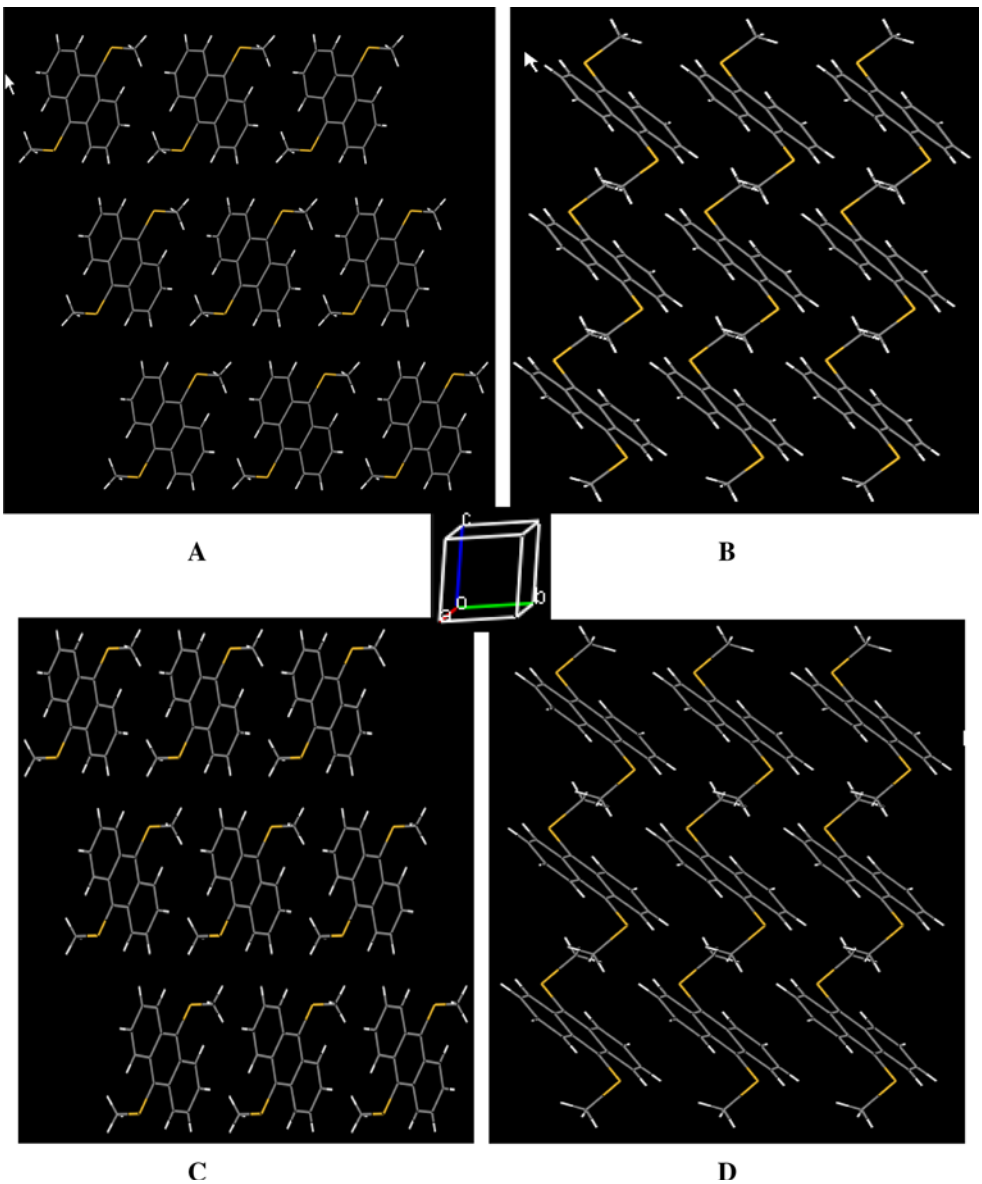

Fig. 3 The experimental (**a** and **b**) and simulated (**c** and **d**) crystal structures of **1** along a and c direction, respectively

appropriate and thus the crystal structures of **2**, **3** and **4** have been simulated by applying the same tactic. Detail about the crystal structures of all the investigated systems in this study can be found in supporting information.

3.2 Charge transfer properties

The anthracene which is used in OFET is a hole transfer material. Bredas et al. [14] calculated its reorganization energies by potential energy surfaces (PES) ($\lambda_h = 0.137$ eV) and normal mode (NM) ($\lambda_h = 0.136$ eV) analyses. They performed all the calculations including geometry optimizations and NM analyses at the DFT level with the hybrid B3LYP functional using 6-31G** basis set. We have calculated the reorganization energy of anthracene at B3LYP/6-31G*,B3LYP/6-31G**, and B3LYP/6-31 + G* levels. From Table 2 it can be found that basis set has no significant effect. Thus, the reorganization energies of anthracene derivatives have been computed at B3LYP/6-31G* level of theory.

On the basis of the crystal structures of **1**, **2**, **3**, and **4**, we identified 13 distinct nearest-neighbor hopping pathways for each investigated system (see supporting information for details). Using the method described above in Eq. 4, the corresponding coupling integrals were calculated for hole and electron. The strongest nearest-neighbor electronic coupling of anthracene is as high as 44 meV [14], while largest coupling for **1** is 35.9 meV for hole and 106 meV for electron when S to S distance is 5.195 Å. The prevailing couplings for hole are 4.9, 10.8, 19, 12, and 5 meV for routes 3, 4, 9, 11, and 12, respectively. The electron couplings for the same routes have been observed 19, 0.6, 9.9, 13, and 2.7 meV, respectively (see Table 3). Generally, reorganization energy indicated that **1** would be hole transfer material while transfer integrals showed that it is electron transfer one. By considering both the reorganization energy and transfer integrals it might be good material for both hole and electron transfer. From Table 4 it can be found that the dominant pathway in **2** is also route 1 when S to S distance is 5.491 Å with $V_h = 133.6$ meV and $V_e = 29.9$ meV. The hole/electron transfer integrals for routes 3, 4, 9, 11, and 12 are 3.6 meV/2.4 meV, 0.48 meV/1.2 meV, 8.7 meV/3.9 meV, 0.45 meV/1.7 meV, and 3.9 meV/0.34 meV, respectively. The computed λ_h is 0.2 eV and λ_e is 0.340 eV. The reorganization energy and transfer integrals showed that it would be hole transfer material. The transfer integrals of **3** are given in Table 5; the main hole couplings are 28.5 meV (route 1), 1.1 meV (route 3), 11 meV (route 4), 17 meV (route 9), 5.4 meV (route 11), and 1.4 meV (route 12) while electron coupling are 40.3 meV (route 1), 6.0 meV (route 3), 3.9 meV (route

Table 2 The calculated reorganization energies for hole (λ_h) and electron (λ_e) in eV

Complexes	B3LYP/6-31G*		B3LYP/6-31G**		B3LYP/6-31 + G*	
	λ_h	λ_e	λ_h	λ_e	λ_h	λ_e
Anthracene[a]	0.136	0.196	0.137	0.195	0.133	0.194
1	0.161	0.216				
2	0.200	0.340				
3	0.214	0.230				
4	0.209	0.331				

[a] The calculated reorganization energies by potential energy surfaces (PES) ($\lambda_h = 0.137$ eV) and normal mode (NM) ($\lambda_h = 0.136$ eV) from [14]

Table 3 The transfer integrals V (eV) of 9,10-bis(methylthio)anthracene (**1**) for the 13 pathways are calculated at the pw91pw91/6-31G* level

Route	S to S distance (Å)	V_h	V_e
1	5.195	-3.59×10^{-2}	10.65×10^{-2}
2	9.071	6.70×10^{-7}	3.43×10^{-6}
3	7.458	4.9×10^{-3}	1.93×10^{-2}
4	9.107	-1.08×10^{-2}	-5.81×10^{-4}
5	13.188	2.43×10^{-20}	2.66×10^{-20}
6	13.173	-5.15×10^{-15}	4.55×10^{-14}
7	15.070	-1.74×10^{-12}	-7.81×10^{-12}
8	9.042	-4.39×10^{-4}	2.84×10^{-5}
9	9.002	-1.90×10^{-2}	-9.90×10^{-3}
10	11.588	4.56×10^{-5}	-8.60×10^{-6}
11	10.043	-1.20×10^{-2}	1.30×10^{-2}
12	9.990	5.00×10^{-3}	-2.70×10^{-3}
13	12.358	6.42×10^{-7}	3.81×10^{-6}

Table 4 The transfer integrals V (eV) of 9,10-bis(trifluoromethylthio) anthracene (**2**) for the 13 pathways are calculated at the pw91pw91/6-31G* level

Route	S to S distance (Å)	V_h	V_e
1	5.491	13.36×10^{-2}	2.99×10^{-2}
2	8.928	2.59×10^{-7}	1.47×10^{-6}
3	7.653	-3.60×10^{-3}	2.40×10^{-3}
4	9.885	4.79×10^{-4}	1.20×10^{-3}
5	14.432	-9.92×10^{-22}	1.32×10^{-19}
6	14.184	4.44×10^{-16}	2.15×10^{-14}
7	15.949	-9.08×10^{-17}	-4.60×10^{-16}
8	10.442	6.54×10^{-5}	-5.53×10^{-6}
9	9.640	-8.70×10^{-3}	-3.90×10^{-3}
10	11.710	-3.99×10^{-5}	-2.31×10^{-5}
11	11.265	-4.55×10^{-4}	1.70×10^{-3}
12	10.090	-3.90×10^{-3}	3.41×10^{-4}
13	11.705	-1.01×10^{-6}	-1.32×10^{-7}

Table 5 The transfer integrals V (eV) of 9,10-bis(methylselleno)anthracene (**3**) for the 13 pathways are calculated at the pw91pw91/6-31G* level

Route	Se to Se distance (Å)	V_h	V_e
1	6.153	2.85×10^{-2}	4.03×10^{-2}
2	9.694	-7.95×10^{-7}	-2.22×10^{-6}
3	7.318	1.10×10^{-3}	-6.00×10^{-3}
4	9.426	1.10×10^{-2}	3.90×10^{-3}
5	12.244	7.72×10^{-18}	5.85×10^{-18}
6	12.188	5.17×10^{-15}	1.51×10^{-13}
7	14.929	-3.16×10^{-12}	-1.07×10^{-10}
8	8.522	2.05×10^{-5}	1.54×10^{-5}
9	8.591	-1.70×10^{-2}	4.50×10^{-3}
10	12.276	2.83×10^{-5}	-2.63×10^{-5}
11	10.121	-5.40×10^{-3}	5.80×10^{-3}
12	10.305	-1.40×10^{-3}	-7.37×10^{-4}
13	13.625	-4.90×10^{-8}	5.05×10^{-8}

Table 6 The transfer integrals V (eV) of 9,10-bis(trifluoromethylselleno)anthracene (**4**) for the 13 pathways are calculated at pw91pw91/6-31G* level

Route	Se to Se distance (Å)	V_h	V_e
1	5.628	6.59×10^{-2}	8.38×10^{-2}
2	9.348	1.04×10^{-7}	5.33×10^{-7}
3	7.848	-4.80×10^{-3}	1.80×10^{-3}
4	9.957	-5.71×10^{-5}	9.38×10^{-4}
5	13.830	-1.21×10^{-20}	3.98×10^{-20}
6	13.626	2.34×10^{-16}	1.83×10^{-14}
7	15.603	-8.54×10^{-16}	-2.38×10^{-15}
8	9.923	1.01×10^{-4}	-6.51×10^{-6}
9	9.328	-9.90×10^{-3}	-5.20×10^{-3}
10	11.785	-7.83×10^{-5}	-7.00×10^{-5}
11	11.352	3.87×10^{-4}	2.20×10^{-3}
12	10.561	1.20×10^{-3}	3.42×10^{-4}
13	12.551	-1.35×10^{-8}	1.65×10^{-7}

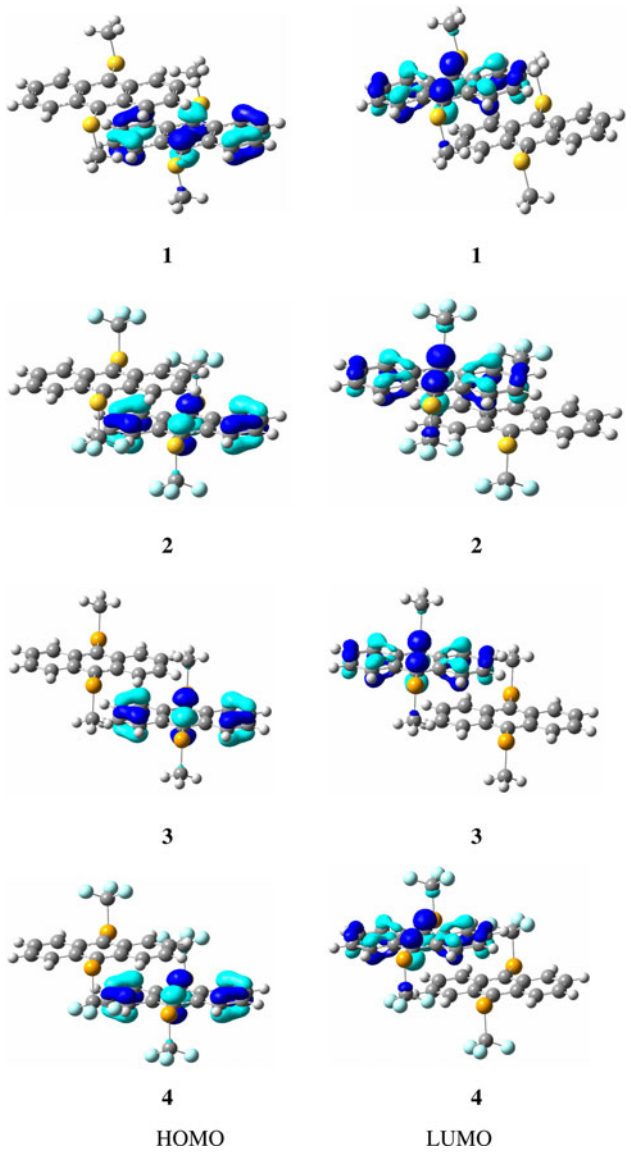

Fig. 4 The molecular orbital distribution of the most prominent dimers

4), 4.5 meV (route 9), 5.8 meV (route 11), and 0.73 meV (route 12). The reorganization energy and transfer integrals showed that **3** would be good for both hole and electron transfer. The key hole couplings for **4** are 65.9, 4.8, 9.9, and 1.2 meV while electron couplings are 83.8, 1.8, 5.2, and 0.34 meV when Se to Se distances are 5.628 Å, 7.848 Å, 9.328 Å, and 10.561 Å, respectively, which are given in Table 6. The hole reorganization energy is smaller than the electron one while electron couplings are higher than hole couplings. It might be better for both hole and electron transfer. The four crystal structures are very closely related; but we have observed that within the same pathway by changing the substituents transfer integral values differs (see Tables 3, 4, 5 and 6). The molecular orbital distribution of the most prominent dimers in **1**, **2**, **3,** and **4** has been shown in Fig. 4. Here, we found that in all the studied systems, HOMOs are localized on one molecule that is below while LUMOs are on other molecule above one.

Electrostatic surface potentials (see Fig. 5) indicate that electron density in **1** is distributed in the central part, but by substituting the fluoro atoms it decreases in the center. The fluoro atoms attract the electrons toward themselves, thus rendering center of the rings in electron-deficient while location of fluorine atoms are electron rich as in **2** and **4**. It might make oxidation more difficult and improve the photostability [22].

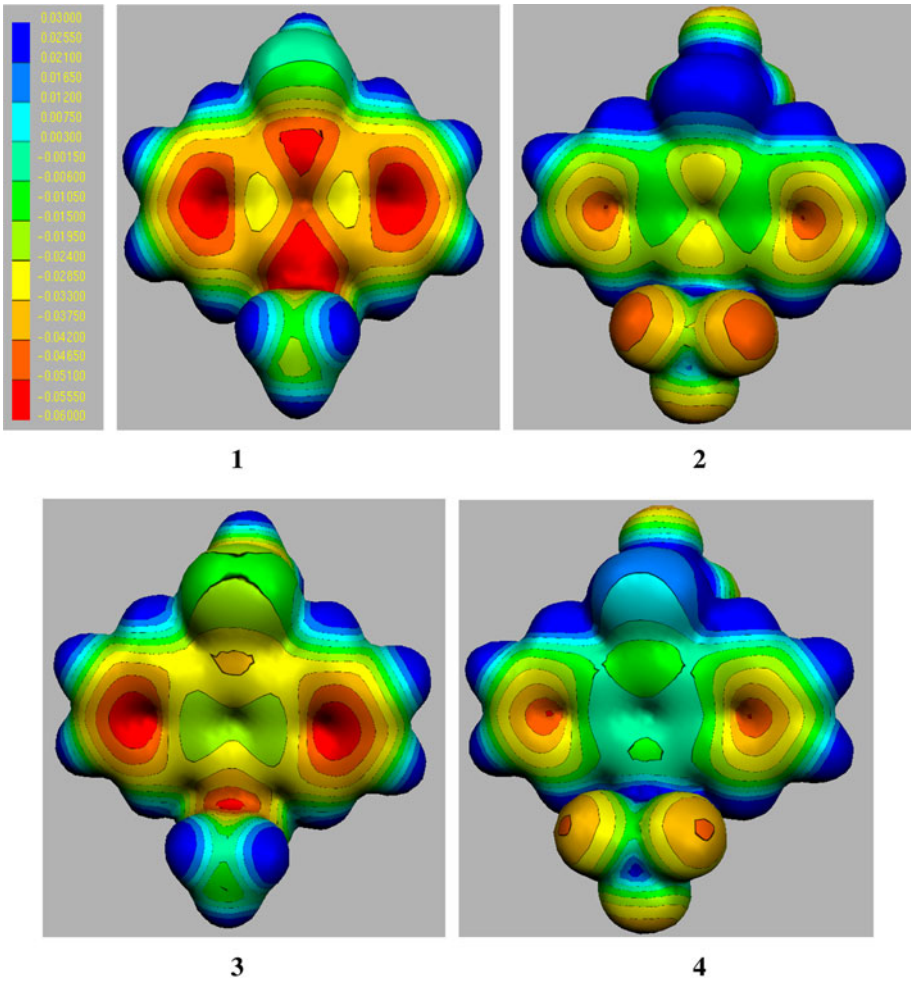

Fig. 5 Electrostatic surface potentials mapped onto a surface of total electron density for anthracene derivatives. Regions of higher electron density are shown in *red* and of lower electron density in *blue* (values in atomic units)

4 Conclusions

The crystal structures of 9,10-bis(methylthio)anthracene (**1**) and new designed derivatives 9,10-bis(trifluoromethylthio)anthracene (**2**), 9,10-bis(methylselleno)anthracene (**3**) and 9,10-bis(trifluoromethylselleno)anthracene (**4**) have been simulated. The intermolecular electronic couplings for a wide variety of nearest-neighbor charge transfer pathways have been obtained by directly evaluating the dimer Fock matrix with unperturbed monomer's molecular orbits at the DFT/pw91pw91/6-31G* level. The 9,10-bis(methylthio)anthracene (**1**) might be good material for both hole and electron transfer. The hole reorganization energy of **2** is lower while hole transfer integral values are higher than the electron ones which indicate that it would be hole transfer material. The reorganization energies and transfer integrals showed that **3** and **4** might be also good for both hole and electron transfer. The electrostatic surface potentials showed that **2** and **4** would be more photostable. Theoretical calculations confirm that investigated system would be excellent potential candidates for OFETs.

Acknowledgments Financial supports from the NSFC (No.50873020; 20773022), NCET-06-0321, and NENU-STB07007 are gratefully acknowledged. A. Irfan acknowledges the financial support from China Scholarship Council and Ministry of Education (MOE), Pakistan.

References

1. Horowitz G, Hajlaoui ME (2000) Adv Mater 12:1046
2. Huitema HEA, Gelinck GH, van der Putten JBPH, Kuijk KE, Hart CM, Cantatore E, de Leeuw DM (2002) Adv Mater 14:1201
3. Halls JJM, Walsh CA, Greenham NC, Marseglia EA, Friend RH, Moratti SC, Holmes AB (1995) Nature 376:498
4. Brabec CJ, Sariciftci NS, Hummelen JC (2001) Adv Funct Mater 11:15
5. Tsumura A, Koezuka H, Ando T (1986) Appl Phys Lett 49:1210
6. Kuszman A, Kapovits L (1985) In: Csizmadia IG, Mangini A (eds) Organic sulfur chemistry: theoretical and experimental advances. Elsevier, Amsterdam, p 191
7. Sudha N, Singh HB (1994) Coord Chem Rev 135–136:469
8. Takimiya K, Kunugi Y, Konda Y, Niihara N, Otsubo T (2004) J Am Chem Soc 126:5084
9. Janzen DE, Burand MW, Ewbank PC, Pappenfus TM, Higuchi H, da Silva Filho DA, Young VG, Bredas JL, Mann KR (2004) J Am Chem Soc 126:15295

10. Bushey ML, Nguyen TQ, Zhang W, Horoszewski D, Nuckolls C (2004) Angew Chem Int Ed 43:5446
11. Wurthner F (2001) Angew Chem Int Ed 40:1037
12. Fritz SE, Martin SM, Frisbie CD, Ward MD, Toney MF (2004) J Am Chem Soc 126:4084
13. Kobayashi K, Masu H, Shuto A, Yamaguchi K (2005) Chem Mater 17:6666
14. Bredas JL, Beljonne D, Coropceanu V, Cornil J (2004) Chem Rev 104:4971
15. Coropceanu V, Cornil J, da Silva Filho DA, Olivier Y, Silbey R, Bredas JL (2007) Chem Rev 107:926
16. Cornil J, Lemaur V, Calbert JP, Bredas JL (2002) Adv Mater 14:726
17. Andrienko D, Kirkpatrick J, Marcon V, Nelson J, Kremer K (2008) Phys Stat Sol b 245:830
18. He YH, Hui RJ, Yi YP, Shuai ZG (2008) Chin J Chem 26:1005
19. Myerson AS (1999) Molecular modeling applications in crystallization. Cambridge University Press, New York
20. van Langevelde A, Capkova P, Sonneveld E, Schenk H, Trchova M, Ilavsky M (1999) J Synchrotron Radiat 6:1035
21. Liu YH, Xie Y, Lu ZY (2009) Chem Phys. doi:10.1016/j.chemphys.2009.11.015 (in press)
22. Yang GY, Hanack M, Lee YW, Chen Y, Lee MKY, Dini D (2003) Chem Eur J 9:2758
23. Becke AD (1993) J Chem Phys 98:5648
24. Lee C, Yang W, Parr RG (1988) Phys Rev B 41:785
25. Stephens PJ, Devlin FJ, Chabalowski CF, Frisch MJ (1994) J Phys Chem 98:11623
26. MS Modeling, Release 3.0.1. (2004) Accelrys Inc., San Diego, CA
27. Liu JX, Dong M, Qin ZF, Wang JG (2004) J Mole Struct Theochem 679:95
28. Klemm E, Wang JG, Emig G (1998) Micropor Mesopor Mater 26:11
29. Fried JR, Weaver S (1998) Comp Mater Sci 11:277
30. Mayo SL, Olafson BD, Goddard WA (1990) J Phys Chem 94:8897
31. Ewald PP (1921) Ann Phys 64:253
32. Marcus RA, Sutin N (1985) Biochim Biophys Acta 811:265
33. Gruhn NE, da Silva Filho DA, Bill TG, Malagoli M, Coropceanu V, Kahn A, Brédas JL (2002) J Am Chem Soc 124:7918
34. Reimers JR (2001) J Chem Phys 115:9103
35. Irfan A, Cui RH, Zhang JP (2009) Theor Chem Acc 122:275
36. Coropceanu V, Nakano T, Gruhn NE, Kwon O, Yade T, Katsukawa K, Brédas JL (2006) J Phys Chem B 110:9482
37. Soos ZG, Tsiper EV, Painelli A (2004) J Lumin 110:332
38. Tsiper EV, Soos ZG (2003) Phys Rev B 68:085301
39. Tsiper EV, Soos ZG, Gao W, Kahn A (2002) Chem Phys Lett 360:47
40. Lin BC, Cheng CP, You ZQ, Hsu CP (2005) J Am Chem Soc 127:66
41. Troisi A, Orlandi G (2001) Chem Phys Lett 344:509
42. Yin SW, Yi YP, Li QX, Yu G, Liu YQ, Shuai ZG (2006) J Phys Chem A 110:7138
43. Valeev EF, Coropceanu V, da Silva Filho DA, Salman S, Bredas JL (2006) J Am Chem Soc 128:9882
44. Yang XD, Li QK, Shuai ZG (2007) Nanotechnology 18:424029
45. Song YB, Di CA, Yang XD, Li SP, Xu W, Liu YQ, Yang LM, Shuai ZG, Zhang DQ, Zhu DB (2006) J Am Chem Soc 128:15940
46. Wang CL, Wang FH, Yang XD, Li QK, Shuai ZG (2008) Org Electron 9:635
47. Kwiatkowski JJ, Nelson J, Li H, Bredas JL, Wenzel W, Lennartzd C (2008) Phys Chem Chem Phys 10:852
48. Huang JS, Kertesz M (2004) Chem Phys Lett 390:110
49. Wang LJ, Nan GJ, YangD X, Peng Q, Li QK, Shuai ZG (2010) Chem Soc Rev 39:423
50. Yang XD, Wang LJ, Wang CL, Long W, Shuai ZG (2008) Chem Mater 20:3205
51. Nan GJ, Wang LJ, Yang XD, Shuai ZG, Zhao Y (2009) J Chem Phys 130:024704
52. Deng WQ, Goddard WA III (2004) J Phys Chem B 108:8614
53. Frisch MJ et al (2003) Gaussian 03, Revision A. 1. Gaussian, Pittsburgh